Fire Safety Journal 119 (2021) 103257

Contents lists available at ScienceDirect

Fire Safety Journal

journal homepage: http://www.elsevier.com/locate/firesaf

Ignition/non-ignition phase transition: A new critical heat flux estimation method

F.Z. Sabi [a], S.M. Terrah [a], O. Mosbah [a], A. Dilem [a], N. Hamamousse [a,b], A. Sahila [a], O. Harrouz [a], H. Boutchiche [a], F. Chaib [a], N. Zekri [a,*], A. Kaiss [b], J.-P. Clerc [b], F. Giroud [c], D.X. Viegas [d]

[a] Université des Sciences et de la Technologie d'Oran, LEPM BP 1505 El Mnaouer Oran, Algeria
[b] Aix Marseille Université, CNRS, IUSTI UMR 7343, 13453, Marseille, France
[c] CEREN, Domaine de Valabre, 13120, Gardanne, France
[d] ADAI, CEIF, University of Coimbra, Portugal

ARTICLE INFO

Keywords:
Critical heat flux for ignition
Phase transitions
Power-law behavior
Ignition probability

ABSTRACT

Flaming ignition properties of dead and live thin wildland porous fuels submitted to different incident heat flux intensities are examined experimentally using a cone calorimeter. Data are compared to analytical and numerical results of a model that uses an energy balance and includes energy and temperature ignition criteria. The model provides the linear trend of ignition time for large heat flux intensities, but fails to reproduce the behavior of data near threshold ignition, because it does not include explicitly volatiles emission at pyrolysis. A new method is proposed for the estimation of the critical heat flux for ignition of porous fuels, based on the ignition time behavior as a power-law that characterizes phase transitions theory. The critical heat flux for ignition thus estimated has been found small compared to literature data. The discrepancy is due to the probabilistic ignition behavior observed in the critical region and ignored by literature that uses deterministic methods for the estimation of the critical heat flux for ignition. The heterogeneities of fuel particles composition and arrangement could be the major causes of such a probabilistic aspect.

1. Introduction

A substance exposed to a heat flux that raises its temperature emits flammable gases that may lead to its ignition. There are flaming or smoldering ignition types that are functions of both gas and solid phase chemistry [1]. While spontaneous ignition is rare and requires high flux intensities to occur [2], piloted ignition is prevalent in wildland fires and requires the aid of ignition sources (e.g. flame, firebrand or spark). Sustained flaming ignition (fire point) is the onset of near-stoichiometric burning with a diffusion flame [3,4]. Ignition time is one of the parameters characterizing the fuels flammability. In thermal ignition theory, ignition time can be expressed analytically for both thin and thick fuels [3]. In the limit of large incident heat flux intensities ignition time behaves inversely with the flux for thin fuels, while for thick fuels it behaves inversely with the square of the flux. As stated by Drysdale [5], the flame is a gas phase phenomenon, where emitted volatiles can be either in the flame state if ignition occurs (finite ignition time) or remain in their gaseous state if ignition does not (infinite ignition time).

Phase transitions are among the most recurrent phenomena in nature. They are understood in thermodynamics as the abrupt or continuous transformation of a system from one phase or state of matter to another. They can be observed in various fields like conductor/insulator or percolation [6], liquid/gas [7] and paramagnetic/ferromagnetic transitions [8,9]. For all these phenomena, any physical quantity A either diverges or vanishes according to a universal power-law formula when the control parameter X tends to its threshold (critical) value X_c [8,10]:

$$A \sim (X - X_c)^{\pm\gamma} \tag{1}$$

Nomenclature

$c_p^{i=f,w}$	specific heat (J/kg.K)	*eff*	effective
DSC	Differential Scanning Calorimetry	*ign*	ignition/ignited tests
e	thickness (m)	*inc*	incident
E_{ign}	critical ignition energy (kJ/m^2)	*lost*	lost
Eu	Eucalyptus	*max*	maximum

(*continued on next page*)

* Corresponding author.
E-mail address: nouredine.zekri@univ-usto.dz (N. Zekri).

https://doi.org/10.1016/j.firesaf.2020.103257
Received 15 April 2020; Received in revised form 5 November 2020; Accepted 15 November 2020
Available online 21 November 2020

(*continued*)

h_c	convection coefficient (W/m^2.K)	*mix*	mixture
h_w	fuel moisture content	*pyr*	pyrolysis
L_w	water latent heat at 373 K (J/kg)	*test*	tests
$m_{i=dry,w}$	mass (kg)	*w*	water
$N_{i=ign,test}$	number of	*0*	ambient
p	asymptotic probability	*Superscripts*	
Ph	Pinus halepensis	*f*	fuel
P_{ign}	ignition probability	*w*	water
$q''_{i=c,\ eff,\ inc,\ lost}$	heat flux (kW/m^2)	*Greek*	
Q''_c	evaporation critical flux (kW/m^2)	Δ	standard deviation
S	base area of sample holder (m^2)	$\delta q''$	width of the critical region (kW/m^2)
$t_{i=chem,ign,\ mix,\ pyr}$	time (s)	ε_{fb}	fuel bed emissivity
$T_{i=0,max,pyr}$	temperature (K)	γ	critical exponent
TGA	Thermal Gravimetry Analysis	ρ	density (kg/m^3)
Subscripts		σ	Stefan-Boltzmann constant (W/m^2.K^4)
c	critical	τ	relaxation time of dry fuel (s)
chem	chemical reaction (combustion)	τ'	relaxation time of moist fuel (s)
dry	dry	φ	packing ratio

Phase transitions characterized by the same critical exponent γ are said to belong to the same class of universality, and are expected to behave similarly even for different phenomena [8,10]. Ignition/non-ignition phase transition is here referred to the different states of the gas phase: flame (ignitable) or gas (non-ignitable). The physical quantities involved in this transition are thus expected to follow the universal power-law behavior in (1) predicted by the theory of phase transitions. If the physical quantity A is ignition time, and the incident flux q''_{inc} is the control parameter X with a threshold value q''_c, the power-law equation (1) becomes:

$$t_{ign} \propto (q''_{inc} - q''_c)^{-\gamma} \tag{2}$$

The power-law formula (2) has been indirectly used for the estimation of the critical heat flux for ignition of thin fuels using cone calorimeter tests [11,12]. The linear trend of the inverse ignition time observed for large heat flux intensities was extrapolated to low flux intensities, which assumes a power-law behavior like in (2) with an exponent $\gamma = 1$. On the other hand, Babrauskas compared a large number of data sets on the piloted ignition of wood specimens (thick fuels) in various orientations and heating conditions [13]. He found a power-law behavior equation (2) with an exponent $\gamma = 1.828$. The power-law behavior in (2) is thus expected to occur at low incident heat flux intensities both for thin and thick fuels. The theory of phase transitions predicts also an enhancement of disorder in the critical region [6,8,10] that leads to failed tests [14], and suggests a probabilistic process. Hence, the estimation of the critical heat flux for ignition using the deterministic methods (ASTM 1354 standard) [15] is questionable. Disorder effect is also present for large heat flux intensities and induces fluctuations of ignition time (see for example the top Fig. 1 of [16]).

The critical heat flux for ignition is an important property that allows wildland managers and firefighters control the fire spread by managing the wildland fuel properties, or using retardants so that the front heat flux intensities remain close to their threshold values. This flammability condition was also subject of scientific interest for several decades (see Refs. [11,12,17–20]). The threshold heat flux value q''_c depends on the heat transfer, weather conditions and fuel properties (nature, ignition temperature, porosity, compactness and moisture content) [21–23]. According to Rothermel, wildland fires with dead fuels will not spread above some threshold value of fuel moisture content [24] (typically assumed to be between 10% and 40%). Recently, no critical moisture content for ignition was observed [25].

The present work focuses on ignition/non-ignition phase transition of live and dead Mediterranean porous fuels by studying the ignition time variation with the incident heat flux. Experimental data from a cone calorimeter are compared to model results based on energy conservation for thermally thin fuels. Although more sophisticated ignition models can be adopted [26], this model was chosen because it has been used to validate several historical and experimental wildland fire spread [27,28]. Using the power-law formula (2), the threshold value of incident heat flux is estimated from experimental data. The probabilistic aspect of ignition is also experimentally investigated in the critical region.

2. Experimental setup

Vegetation samples (needles or leaves) of 10 *g* mass are placed in a cylindrical holder of a mesh shape of 10 *cm* diameter and 5 *cm* height with sample thicknesses in the range $0.9 - 1.1$ *cm*. The corresponding fuel load is 1.27 kg/m^2. For the probabilistic study of ignition, samples of *Ph* needles of mass 15 *g* (with thicknesses lying in the range $1.2 - 1.5$ *cm*) are used for comparison with those of mass 10 *g*. An example of vegetation sample is presented in Fig. 1a. Particles are assumed to be thermally thin with leaves thickness or needles diameter of less than 1 *mm*.

The sample is exposed to a constant radiative heat flux provided by the heat source of a cone calorimeter with an electrical resistance of 3000 W nominal power. It is placed at different distances from the heat source, so that it receives radiation heat flux magnitudes ranging from 9 to 25 kW/m^2 at its center (see Fig. 1b). The incident heat flux at top surface center position of the sample is calibrated using a water-cooled heat flux sensor of type Hukseflux SBG 01 working in the range $0 - 200\ kW/m^2$. The homogeneity of the incident heat flux in the sample is

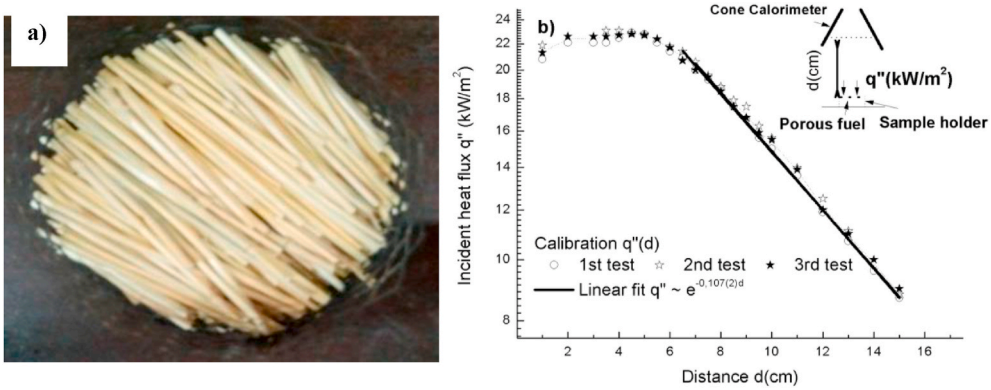

Fig. 1. a) a picture of straw in the holder as an example of fuel sample. b) A schematic representation of the calibration flux and the experimental setup.

not affected by varying the distance to the cone. Using the above mentioned heat flux sensor, it is found that the ratio of the flux intensity at center to the average one is 1.006 at a distance of 2.5 *cm* from the bottom of the cone, and is 1.04 at a distance of 15 *cm*. This ratio is smaller than 1.06, which meets the uniformity requirement ISO 5660–1 [29]. The ignition process is controlled by a pilot flame located 1 *cm* above the sample top surface according to ASTM 1354 standards [15], and the ignition time is recorded. The fuel moisture content is here defined on dry basis:

$$h_w = \frac{m_w}{m_{dry}} \tag{3}$$

It was determined by oven drying both in a microwave and desiccator. Three different species of vegetation were used: *Ph* needles (fresh live fuel) harvested and ignited in January 2018, straw needles (dead fuel dried naturally) ignited in July 2018, and *Eu* leaves (fresh live fuel) harvested and ignited in August 2018. In order to neglect chemical composition changes and to guarantee the live character of *Ph* and *Eu* samples, vegetation particles are harvested and ignited within the same day. The ignition test is accounted successful if the flame persistence time is greater than 4 *s*. We consider that ignition did not occur if the smoldering combustion is observed with a complete oxidation of the fuel in its solid phase [30]. The time of exposition to the heat flux varies from a test to another, with a maximum time of 75 *min*.

Due to the heterogeneity of the sample structure, five (5) ignition tests were realized for each value of the incident heat flux for repeatability. In the region of low heat flux intensities (close to the threshold value) some ignition tests failed and more tests were required as to fulfill the five successful ignitions condition. In order to investigate the probabilistic aspect of ignition, 50 tests were performed for each heat flux condition. The tests were conducted in a draft-free room with temperatures and relative humidity respectively in the ranges of 13-19°C, and 50 – 60% for *Ph* needles and 20-30°C and 45 – 55% for straw and *Eu* leaves.

3. Model description

As mentioned above, the present model is based on the energy conservation. It has been used to describe ignition process [3,28], and has been also included in the *Small World Network* model of fire spread that validated historical and experimental fires [27]. This model is applied here to the cone calorimeter experimental setup (Fig. 1b), where a porous sample composed of thin particles (Fig. 1a) is submitted to a constant heat flux q''_{inc} provided by the cone heater. Piloted ignition occurs if the surface temperature of the sample reaches the pyrolysis temperature (T_{pyr}). Here the gradient temperature of the sample particles (considered as thin) is neglected, and in-depth temperature can be represented by surface temperature. Ignition time is usually expressed as the sum of times of different processes assumed to not occur simultaneously [3]:

$$t_{ign} = t_{pyr} + t_{mix} + t_{chem} \tag{4}$$

Usually the time for fuel/oxygen mixture to reach pilot, and that for the mixture to proceed to combustion are sufficiently small to be neglected compared to t_{pyr}. Three ignition criteria are known for constant irradiation flux: the critical temperature, the critical energy and the critical mass loss rate [31]. As pyrolysis temperature is the condition of ignition, only the critical temperature (T_{pyr}) is considered in this model. The effective heat flux q''_{eff} absorbed by the fuel sample is:

$$q''_{\mathrm{eff}} = q''_{\mathrm{inc}} - q''_{\mathrm{lost}} \tag{5}$$

Neglecting the conductive heat transfer in thermally thin approximation, the heat flux lost from the sample is composed of a radiative and a convective part:

$$\mathrm{q}''_{\mathrm{lost}} = \mathrm{h_c}(\mathrm{T} - \mathrm{T_0}) + \sigma\,\varepsilon_{\mathrm{fb}}\left(\mathrm{T}^4 - \mathrm{T}_0^4\right) \tag{6}$$

The energy accumulated by a thin solid sample during its ignition delay is assumed to allow surface temperature reach pyrolysis temperature T_{pyr} in three steps: i) the temperature raise of moist sample up to boiling (373 K), ii) the evaporation of water from moist sample at boiling temperature, iii) the temperature raise of dried sample up to T_{pyr}. Neglecting the heat of water desorption, the energy conservation for a solid fuel in the thermally thin approximation is:

$$\int_0^{t_{ign}} \mathrm{q}''_{\mathrm{eff}}\,\mathrm{S}\,\mathrm{dt} = \begin{cases} \displaystyle\int_{\mathrm{T_0}}^{373\ \mathrm{K}} \left(\mathrm{m_{dry}c_p^f} + \mathrm{m_w c_p^w}\right)\mathrm{dT} \\ \displaystyle\int_{\mathrm{m_w}}^{0} \mathrm{L_v dM} + \\ \displaystyle\int_{373\ \mathrm{K}}^{\mathrm{T_{pyr}}} \mathrm{m_{dry}c_p^f dT} \end{cases} \tag{7}$$

As the fuel considered here is porous (see Fig. 1a), the effective surface exposed to the heat flux in the holder is different from that of the solid fuel. For a fuel sample with moisture content h_w its mass is related to its density $\rho(h_w)$ as:

$$m(h_w) = \varphi(h_w).\rho(h_w).S.e \tag{8}$$

The packing ratio φ is the ratio of volume of the solid part (particles) to that of the fuel bed for the same mass. This ratio is smaller than one for porous fuels and is unity ($\varphi = 1$) for solid fuels. If the expressions of moisture content h_w in (3) and the dry fuel mass in (8) are included in (7), the energy conservation for porous fuels becomes:

$$\int_0^{t_{ign}} q''_{eff}\,dt = \begin{cases} \displaystyle\int_{T_0}^{373K} \varphi(0)\rho(0)e\left[c_p^f + h_w c_p^w\right]dT - \\ \displaystyle\int_{h_w}^{0} \varphi(0)\rho(0)eL_w dh'_w + \\ \displaystyle\int_{373\ K}^{T_{pyr}} \varphi(0)\rho(0)ec_p^f dT \end{cases} \tag{9}$$

Ignition time is thus the sum of the times involved in the three above mentioned steps leading to equation (9). To solve equation (9) for $T(t)$ and $h'_w(t)$, the following boundary conditions are needed:

$$\begin{aligned} &T(t=0) = T_0; \quad h'_w(T < 373\ K) = h_w \\ &T\left(t = t_{ign}\right) = T_{pyr}; \quad h'_w(T > 373\ K) = 0 \end{aligned} \tag{10}$$

Among the three ignition criteria mentioned above, the critical temperature appears to be the unique criterion used in the model represented by (9). However, the critical energy (second ignition criterion [31]) defined as the total absorbed energy per unit area required for ignition ($E_{ign} = \int_0^{t_{ign}} q''_{eff}\,dt$) appears in the left side of (9). If the fuel parameters are constant, the integration of (9) yields:

$$E_{ign} = \varphi(0)\rho(0)e\left[c_p^f\left(T_{pyr} - T_0\right) + h_w\left\{c_p^w(373 - T_0) + L_w\right\}\right] \tag{11}$$

Hence the model includes both energy and temperature ignition criteria. According to the pyrolysis kinetics assumed by Drysdale (see equations 1.1 and 1.2 of [5]), the critical mass loss rate is expected to be related to T_{pyr} that depends on the heat of gasification (see equation (17) of [4]). The third ignition criterion appears thus implicitly used in the model through the pyrolysis temperature. The critical energy in (11) depends on ambient temperature, critical temperature T_{pyr}, and the physical characteristics of water and fuel, but does not depend on heat transfer mechanism. It is here independent of ignition time contrary to the results of transient irradiations [32], where this energy is square correlated to ignition time. Note that in Ref. [32] the lost heat flux is neglected assuming a low thermal inertia. However, thermal inertia

varies with temperature during pyrolysis due to the increase of heat capacity and mass loss.

The fuel will either ignite or not depending on the intensity of incident heat flux. For sufficiently large heat flux intensities, ignition occurs with a small ignition time. As the intensity of the incident flux decreases, ignition time increases. No ignition occurs (infinite ignition time) for sufficiently low incident heat flux intensities, because the surface temperature never reaches pyrolysis temperature ($T_{max} < T_{pyr}$), and consequently, the total absorbed energy never reaches the critical energy E_{ign} from (11). There exists a critical incident flux intensity q''_c above which ignition occurs. It is defined as the incident flux for which the maximum surface temperature reached asymptotically ($t \to \infty$) coincides with pyrolysis temperature ($T_{max} = T_{pyr}$), or equivalently, the absorbed energy coincides with E_{ign}. The critical heat flux for ignition has been shown to be one of the conditions of sustained piloted ignition (see equation (20) of [4]).This threshold flux is thus the relevant parameter describing the ignition phase transition predicted by (2).

4. Results and discussion

This section aims to compare ignition time results obtained by the current model with experimental data, and to estimate the critical heat flux for ignition q''_c according to the power-law formula (2). Furthermore, the ignition probabilistic process occurring near the critical region is investigated experimentally. Let us first consider a simple case where equation (9) can be solved analytically. This allows examine the trend of the ignition time in terms of $q''_{inc} - q''_c$ near threshold flux.

4.1. Analytical resolution of the model for a simple case

Equation (9) can be solved analytically assuming convective losses heat flux $q''_{lost} \cong h_c(T - T_0)$. This occurs also for radiative losses flux if surface temperature is close to ambient $(T - T_0)/T_0 \ll 1$). Let us first neglect moisture content in (9) that is reduced to a one step integral equation with a continuous surface temperature rise. The corresponding differential equation is a relaxation-like equation with a relaxation time $\tau = \varphi(0)\,\rho(0)\,e\,c_p^f/h_c$:

$$\frac{q''_{inc}}{h_c} - (T(t) - T_0) = \tau \frac{\partial (T(t) - T_0)}{\partial t} \tag{12}$$

The solution of equation (12) (see also in Ref. [3] equation 7.27) is:

$$T(t) - T_0 = \frac{q''_{inc}}{h_c}\left(1 - e^{-t/\tau}\right) \tag{13}$$

In the non-ignition state, the maximum temperature $T_{max} = T_0 + q''_{inc}/h_c \le T_{pyr}$ is reached asymptotically ($t \to \infty$), and corresponds to equilibrium $q''_{inc} = q''_{lost}$. As defined in the previous section, the critical heat flux for ignition is the incident flux for which the asymptotic condition $T_{max} = T_{pyr}$ is satisfied. For dry fuels we have:

$$q''_c = q''_c(h_w = 0) = h_c\left(T_{pyr} - T_0\right) \tag{14}$$

In the ignition state, ignition time is deduced analytically from (13) with $T(t_{ign}) = T_{pyr}$. Using the equation (14), we have:

$$t_{ign}/\tau = ln\left(1 - \frac{q''_c}{q''_{inc}}\right)^{-1} \sim ln(q''_{inc} - q''_c)^{-1} \tag{15}$$

In the limit of sufficiently large intensities of the incident heat flux ($q''_c/q''_{inc} \ll 1$), the logarithmic behavior in (15) is reduced to the inverse linear behavior of ignition time:

$$t_{ign}^{-1} = \frac{1}{\tau}\frac{q''_{inc}}{q''_c} = \frac{1}{\tau}\frac{q''_{inc}}{h_c\left(T_{pyr} - T_0\right)} \tag{16}$$

This linear behavior was deduced previously by Quintiere (see equation 7.28 of [3]), and has been observed experimentally for large intensities of heat flux [11,12]. By taking $h_w = 0$ in (11), the critical energy depends thus on the relaxation time of the heating process and the critical heat flux through the relation $E_{ign} = \tau q''_c$.

Let us now include the contribution of water heating and evaporation on ignition time of moist fuels. In the first step (moist fuel heating), the differential equation involved in (9) remains relaxation-like similarly to equation (12) with a relaxation time $\tau' = \tau(1 + h_w c_p^w/c_p^f)$. The second step is characterized by a critical heat flux for water evaporation $Q''_c = h_c(373 - T_0)$. Solving the differential equations involved in (9) for each step, yields:

$$T(t) - T_0 = \frac{q''_{inc}}{h_c}\left(1 - e^{-t/\tau'}\right) \quad \text{for} \quad T_0 \le T < 373\text{K} \tag{17a}$$

$$h_w(t) = \frac{q''_{inc} - Q''_c}{\varphi(0)\,\rho(0)\,eL_w}t \quad \text{for} \quad T = 373\ K \tag{17b}$$

$$T(t) - T_0 = \frac{q''_{inc}}{h_c}\left(1 - e^{-t/\tau}\right) \quad \text{for} \quad 373\ K \le T < T_{pyr} \tag{17c}$$

The total ignition time is the sum of the times involved in the three processes of ignition (see appendix):

$$t_{ign}/\tau = -\ln\left(e^{-h_w\frac{L_w h_c}{q''_{inc} - Q''_c}/\frac{c_p^f}{c_p^f}}\left(1 - \frac{Q''_c}{q''_{inc}}\right)^{1 + h_w\frac{c_p^w}{c_p^f}} - \frac{q''_c - Q''_c}{q''_{inc}}\right) \tag{18}$$

The logarithmic expression in (15) is recovered here for $h_w = 0$. The critical heat flux for ignition of moist fuels $q''_c(h_w)$ corresponds to the incident flux for which the argument of the logarithmic term of (18) vanishes. In the limit of large intensities of the incident flux ($q''_{inc} \gg q''_c$), and for not very large values of moisture content so that the argument of exponential in (18) remains small, equation (18) can be approximated at first order as:

$$\frac{t_{ign}}{\tau} \approx \left[\left(1 + h_w\frac{L_w}{c_p^f\left(T_{pyr} - T_0\right)}\right)q''_c + h_w\frac{c_p^w}{c_p^f}Q''_c\right]q''^{-1}_{inc} \tag{19}$$

Hence, the inverse ignition time is still linearly varying with the incident heat flux similarly to dry fuels in (16), but with a slope strongly decreasing with moisture content.

However, the model does not include explicitly the contribution of flammable volatiles emission at T_{pyr}. If moisture is neglected ($h_w = 0$) for simplicity, and the emission of volatiles at T_{pyr} is included as in (17b), the critical heat flux for their emission Q''_c would coincide with q''_c defined by (14). Equation (18) becomes:

$$\frac{t_{ign}}{\tau} = \frac{h_v L_v h_c}{c_p^f}\left(q''_{inc} - q''_c\right)^{-1} + \left(1 + h_v\frac{c_p^v}{c_p^f}\right)\ln\left(1 - \frac{q''_c}{q''_{inc}}\right)^{-1} \tag{20}$$

Here L_v and c_p^v are respectively the latent heat and heat capacity of emitted volatiles, and h_v is the mass proportion of volatiles in the fuel. Equation (20) provides a more complete description of ignition, since it includes explicitly the third ignition criterion (the critical mass loss rate due to volatiles emission at pyrolysis). It combines both power-law and logarithmic behavior of ignition time with respect to $q''_{inc} - q''_c$. The power-law trend dominates the divergence near threshold flux. In the next subsection, the critical heat flux for ignition is estimated by assuming the power-law behavior of ignition time for experimental data.

4.2. Model comparison with experimental data

Now let us compare model results to experimental data. Porous fuels composed of thermally thin particles (as shown in Fig. 1a) are submitted to a cone calorimeter providing a constant heat flux (see section 2). The lost heat flux is then dominantly radiative (non-linear with temperature), and thus equation (9) cannot be solved analytically. This equation is then solved numerically using the second order Runge-Kutta method

Table 1
The physical parameters of the fuels used in the model and their moisture content.

Material type	Density ρ	c_p^f at 300 K	h_w from (3)
Water	997.05 [35]	4182 [35]	–
Straw	500 [36]	1700 [37]	0.11
Ph needles	789 [38]	1827 [38]	1.27
Eu leaves	1800 [39]	1547 [40]	1.33

for the parameters shown in Table 1, and using $\varepsilon_{fb} = 0.9$, $L_w = 2.257 \times 10^6 J/kg$ and $T_0 = 298\ K$. As the trends of temperature are similar for the three fuels considered here, only model results for straw are presented to avoid clutter. In order to compare model results with experimental data for straw, two pyrolysis temperatures are considered (410 K and 500 K) in addition to that used by Koo et al. [28] ($T_{pyr} = 561\ K$). The critical temperature for auto-ignition was found to vary from 254 to 530 °C for wood [33], and from 380 to 511 °C for *Cistus Monspeliensis* depending on the particle size [34]. For piloted ignition, the pyrolysis temperature is much smaller.

The temperature evolution, which is a solution of (9), is shown in Fig. 2a for different intensities of the heat flux. Surface temperature follows a relaxation-like trend similarly to equation (13), with a maximum temperature $T_{max} < T_{pyr}$ reached asymptotically in case of non-ignition (i.e. for $q''_{inc} < q''_c$). Ignition occurs when $T_{max} > T_{pyr}$ as shown for $q''_{inc} = 5\ kW/m^2$ in Fig. 2a. Using the above definition of the critical heat flux for ignition of dry fuels (i.e. $T_{max} = T_{pyr}$) yields:

$$q''_c = \sigma \varepsilon_{fb} \left(T_{pyr}^4 - T_0^4 \right) \tag{21}$$

As discussed above, the critical energy depends on the critical heat flux and the relaxation time ($E_{ign} = \tau q''_c$) independently of heat transfer mechanism. Here, temperature evolution exhibits an anomalous relaxation governed by a relaxation equation similar to equation (12), but involving the non-linear term $T^4 - T_0^4$ [41,42]. The relaxation time for such a radiative heat transfer can be deduced using equations (11) and (21).

Experimental data are compared to model results in Fig. 2b, where the inverse of the ignition time is presented as a function of the incident heat flux. For intensities of the flux larger than 16 kW/m^2, a linear trend can be fitted for straw data with a correlation coefficient ($R^2 \approx 0.998$), much better than for *Ph* and *Eu* ($R^2 \approx 0.96$). This trend is predicted analytically from (19) and confirmed by model results. Hence, the critical heat flux for ignition is expected to be much smaller than 16 kW/m^2. Note here the sharp slope for straw data compared to those of *Ph* and *Eu* in Fig. 2b. This can be explained by the small moisture content of straw samples dried naturally ($h_w = 0.11$) compared to that of the other fuels ($h_w > 1$). For not very large moisture content values, the line slope decreases when the moisture content increases, similarly to the trend of (19). High moisture contents lead also to increase the fluctuations of ignition time (as observed for *Ph* and *Eu* data) by either strengthening flammable volatiles emission [23] or by preventing ignition because of the presence of water vapor at pilot. The line slope of straw data at large heat flux intensities ($q''_{inc} > 16\ kW/m^2$) is 0.0131 ± 0.0004 m^2/kJ in Fig. 2b. This value of the slope corresponds to model results with a pyrolysis temperature $T_{pyr} = 325$ K (not shown). No piloted ignition test has been observed experimentally at this surface temperature. In addition, the model at $T_{pyr} = 325$ K yields ignition time values much smaller than those of experimental data. The closest reasonable results to experimental data for straw are those using a pyrolysis temperature of 410 K even if the slope is still small.

As expected, the curves become non-linear for low heat flux intensities. Furthermore, fluctuations of data on ignition time are observed because of the heterogeneous character of fuel bed (not included in the model). The critical heat flux corresponds to the intersection of the curves with horizontal axis ($1/t_{ign} = 0$) in Fig. 2b. This requires the knowledge of q''_c with infinite accuracy. For model results q''_c is given by (21) for dry fuels, but only numerical solutions with values at four digits of precision are shown in Fig. 2b. This corresponds to $|q''_{inc} - q''_c| < 0.1$ W. Sensor's uncertainties for experimental measurements are of 100 W.

The extrapolation to horizontal axis is difficult for experimental data on ignition time because of their fluctuations and non-linear behavior. The present estimation method of the critical heat flux for ignition for the current fuels is based on the phase transitions concepts described by the universal power-law behavior in (2) near threshold flux [6–9] as discussed above. Experimental data and numerical results shown in Fig. 2b are now presented in Fig. 3a in logarithmic scale with respect to $q''_{inc} - q''_c$, where q''_c is an unknown parameter that is varied until the

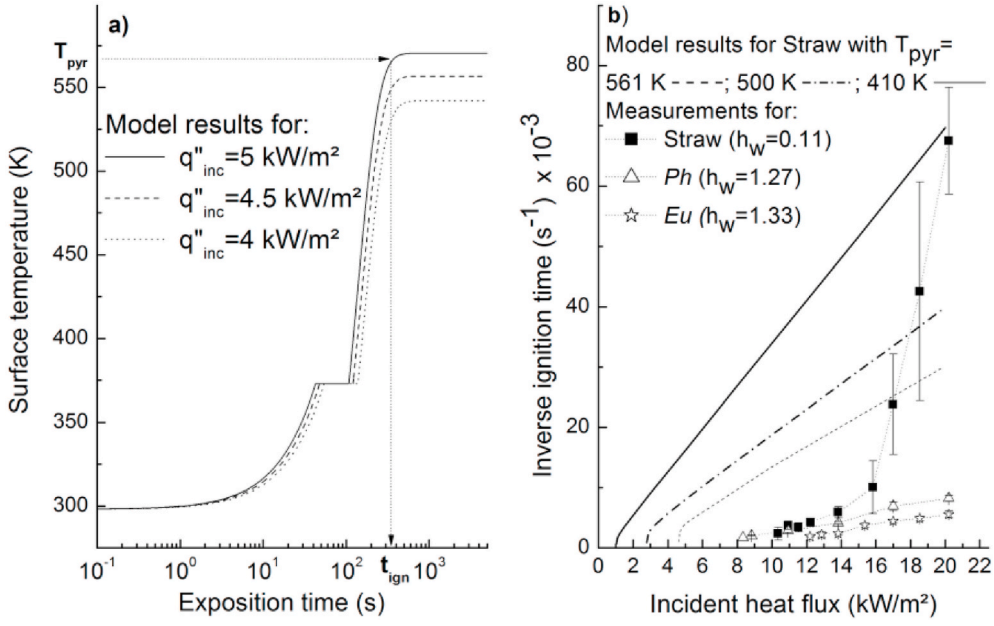

Fig. 2. a) Surface temperature vs. exposition time for various incident flux intensities for straw. b) The inverse ignition time vs. incident heat flux for experimental data and model results.

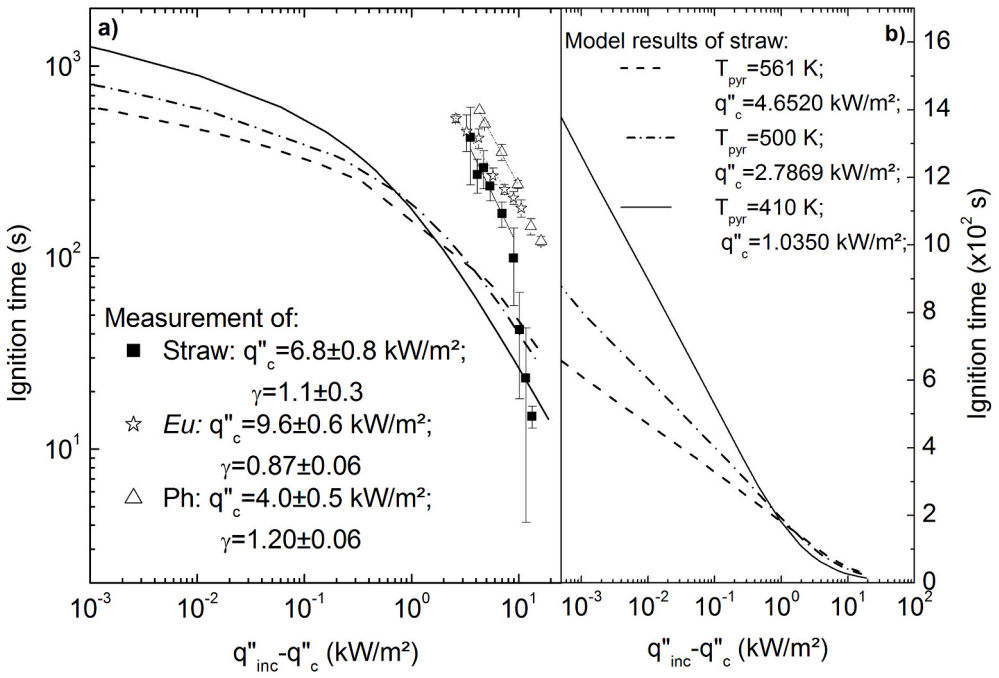

Fig. 3. The ignition time vs. $q''_{inc} - q''_c$ for: a) model results (curves) and experimental data (symbols) in logarithmic scale, b) model results in semi-logarithmic scale.

best power-law fit (appearing as a line) is reached. The best linear fits of data at low heat flux intensities are obtained with correlation coefficients $R^2 > 0.95$ (the fitted parameters appear in Fig. 3a). However, numerical results clearly show a better linear behavior in Fig. 3b, where only the heat flux axis is presented in logarithmic scale, confirming the logarithmic behavior predicted by the model in (18). For numerical results, the values of the critical heat flux determined at four digits precision from Fig. 2b are shown in Fig. 3b. The value at 410 K ($\dot{q}''_c = 1.0395\ kW/m^2$) is very small compared to that estimated for straw data ($\dot{q}''_c = 6.8 \pm 0.8\ kW/m^2$). Hence, the model seems to fail in reproducing data and behavior at low values of the flux. As expected above, clearly the critical heat flux for ignition for straw data is far from the region of linear behavior that begins at 16 kW/m^2 in Fig. 2b.

Now let us compare the values of the critical heat flux and power-law exponent estimated from the fit parameters of data in Fig. 3a. The critical heat flux for ignition appears much larger for *Eu* leaves ($q''_c = 9.6 \pm 0.6\ kW/m^2$) than for straw ($q''_c = 6.8 \pm 0.8\ kW/m^2$) and *Ph* needles ($q''_c = 4.0 \pm 0.5\ kW/m^2$). This confirms the large fire susceptibility index of *Ph* needles observed in the Mediterranean wildlands [43]. *Eucalyptus* leaves are found here less easily flammable, but this fuel contributed significantly to extreme wildfires that occurred in 2017 in Portugal (where it is the major fuel) [44]. Indeed, *Eu* leaves are known to produce a large amount of oils, and *Eu* crown fires spread rapidly [45,46]. It is worth noticing that the value of the critical flux for ignition estimated from data of *Ph* needles appears small compared to that given by literature (around 8 kW/m^2) [38,47]. The values of literature are estimated using a deterministic method according to ASTM 1354 standards [15]. In the concepts of phase transitions on which the present critical flux estimation method is based, a maximum disorder is expected near threshold flux. Ignition tests may thus fail leading to a probabilistic behavior. The other quantity estimated from Fig. 3a is the power-law exponent that corresponds to the line slope. The estimated values of the exponent appear the same for needles within statistical errors ($\gamma = 1.20 \pm 0.06$ for *Ph,* and $\gamma = 1.1 \pm 0.3$ for straw), but they are smaller for *Eu* leaves ($\gamma = 0.87 \pm 0.06$). Hence, needles and leaves ignition phase transition belongs to different classes of universality as defined above [6–9], suggesting different ignition processes. The rate of gas evaporation at ignition depends strongly on the shape, particle arrangement and compactness of the fuel [48]. From recent investigations using electron scanning microscopy, leaves were found to have much more pores than needles [49].

Although the model is successful in describing ignition process [3] and in validating the spread of previous wildfires [24], there are discrepancies with experimental data particularly for low heat flux intensities. These disagreements may be caused by:

a) The lack of use of the third ignition criterion (the critical mass loss rate) in the model [4,31]. If flammable volatiles emission is included in the model (in the second term of equation (9)), ignition time will behave as a power-law in the critical region similarly to equation (20) as observed for experimental data in Fig. 3a.
b) The constant value of fuel heat capacity c_p^f used in the model (see Table 1). This quantity depends on temperature during pyrolysis process.
c) The absence of convection induced by the heat source (e.g. the flames) particularly for fire spread modeling. Such an effect enhances the incident flux, and may explain unexpected wildfire behaviors like junction fires [50,51].
d) The homogeneity of wildland fuels considered in the model, leading to a deterministic ignition process that corresponds to an average ignition time. Hence, the observed fluctuations of ignition time and the failed ignition tests at low intensities of the flux (probabilistic behavior) are not reproduced by the model.

In order to reproduce the ignition time data it is necessary to include the behavior of the above mentioned parameters in the model. However, it is difficult to know for example the temperature dependence of heat capacity and the rate of volatiles emission in the conditions of experimental setup. Concerning heat capacity, its temperature dependence can be measured in laboratory by means of DSC/TGA. A linear temperature dependence of heat capacity was proposed to simulate the ignition process [4]. However, the sharp temperature rise in the conditions of the cone calorimeter may strongly influence its behavior, and non-linear trends might appear for higher temperature rises [52]. Regarding the rate of volatiles emission, its temperature dependence is known only qualitatively especially at high temperatures, where a maximum

emission rate was observed around 175 °C [53]. Before ignition, the mass loss rate is expected to behave with temperature according to an Arrhenius law [5] that could be influenced by the distribution of pores in fuel particles [49]. Finally concerning the last discrepancy point, accounting for the fuel heterogeneity in the model requires the knowledge of fuel distribution in the sample (distribution of packing ratio), and even that of microscopic components in fuel particles. Since the fuel heterogeneity is not included in the model, the probabilistic analysis of ignition is investigated only experimentally in the next subsection for *Ph* fuels.

4.3. Probabilistic effects of the ignition phase transition

As discussed above (see discrepancy d), not all ignition tests may succeed near threshold heat flux. Therefore, additional tests were required to fulfill the five successful ones in Fig. 3a. Similar situations where ignition may succeed or not have been also observed for fuel bed ignition by hot particles that simulate spotting processes near diameter/temperature critical line [54]. The probabilistic ignition behavior appearing in the critical region is most probably caused by the complexity of wildland fuels (e.g. moisture content and random arrangement and compactness of vegetation particles in the sample [24,48]). According to Rothermel [24], there is an optimal packing ratio allowing maximum fire intensity and reaction velocity. It separates oxygen-limited combustion for sufficiently large ratios and fuel-limited combustion for sufficiently small ratios [55]. The packing ratio φ defined by (8) is in fact an average quantity that can be deduced from a distribution of local compactness (throughout the sample). This induces the stochastic behavior of ignition process for porous fuels. The rate of gas emission was found to increase as the incident heat flux increases for solid fuels [56], and is expected to increase also for porous fuels. According to the work of Vermisi et al. [57], the dual threshold condition (critical mass loss rate and critical temperature) must be fulfilled for ignition. For sufficiently large incident heat flux intensities, the distribution of compactness or porosity (for a given packing ratio) leads to fluctuations of ignition time, but both ignition criteria (the critical mass loss rate for sustained ignition [4] and the critical temperature) are always reached. Ignition time is thus the minimum time to reach the dual threshold condition. In contrast, in the critical region both the mass loss rate and temperature fluctuate around their critical values. In this case configurations where at least one of the two threshold conditions is not fulfilled appear, leading to failing tests.

Let us now examine the probabilistic behavior of ignition tests. Ignition probability is defined for each incident heat flux as the ratio of the number of successfully ignited tests to the total number of tests ($P_{ign} = N_{ign}/N_{test}$). This probability is equal to unity for sufficiently large intensities of the flux ($P_{ign}(q''_{inc} \gg q''_c) = 1$), and vanishes for intensities smaller than the threshold flux ($P_{ign}(q''_{inc} < q''_c) = 0$). The critical region for ignition is thus defined as the interval of incident heat flux intensities $\delta q''$ where ignition probability P_{ign} lies in the range $0 < P_{ign} < 1$. The accuracy of the estimated ignition probability depends on the number of tests (N_{test}). For a small number of tests (few tests), the ignition probability distribution is a binomial law (either succeeded or failed ignition). It is expected to become Gaussian [58] and obeys the central limit theorem [59] in the limit $N_{test} \to \infty$. Let p be the limit value of ignition probability for a given intensity of the flux ($P_{ign} = p$ for $N_{test} = \infty$). According to the law of large numbers [58,59], the average number of successfully ignited tests and its variance are respectively $N_{ign} = pN_{test}$, and $\Delta N_{ign}^2 = pN_{test}(1-p)$. Hence, relative fluctuations of the number of ignited tests asymptotically decrease inversely with the square root of the number of tests as:

$$\frac{\Delta N_{ign}}{N_{ign}} = \frac{1}{\sqrt{N_{test}}}\sqrt{\frac{1-p}{p}} \tag{22}$$

Hence, in the limit $N_{test} \to \infty$ the statistical fluctuations of the number of ignited tests vanish. Using (22), the standard deviation of ignition probability for large but finite number of tests is:

$$\Delta P_{ign} = \frac{\Delta N_{ign}}{N_{test}} = \frac{N_{ign}}{N_{test}}\sqrt{\frac{1 - N_{ign}/N_{test}}{N_{ign}}} = P_{ign}\sqrt{\frac{1}{N_{ign}} - \frac{1}{N_{test}}} \tag{23}$$

In Fig. 4, ignition probability is presented as a function of the incident heat flux for *Ph* samples with two values of the mass: 10 g and 15 g (or using equation (8): $\varphi = 0.16$ and 0.20 respectively). A wide range of heat flux intensities is swept including the critical region ($0 < P_{ign} < 1$) with fifty tests ($N_{test} = 50$) for each intensity of the flux. The error bars estimated from (23) are shown in Fig. 4 except for tests with no ignition ($N_{ign} = 0$). The minimum ignition probability that can be measured here is $P_{ign} = 2\%$ (i.e. one successful test). Obviously, from Fig. 4 ignition probability at the estimated critical heat flux $q''_c = 4.0 \pm 0.5$ kW/m^2 is expected to be much smaller than this limit probability. The ignition probability at ($q''_c = 4.0 \pm 0.5$ kW/m^2) would correspond to the limit probability for $N_{test} = \infty$. The values of the critical heat flux for ignition presented in literature [38,47] were estimated according to ASTM 1354 standards [15] with only few tests (at most 5 tests for repeatability). These values are consistent with the value of the heat flux corresponding to $P_{ign} \cong 20\%$ in Fig. 4. Hence, the difference between the value of the critical heat flux for ignition estimated from Fig. 3a and that given by literature is mainly due to the probabilistic behavior of ignition, ignored by the methods of literature. Deterministic methods thus over-estimate threshold heat flux, since there are still configurations where the fuel can be ignited. The threshold flux estimated from Fig. 3a appears then much more accurate for fire safety purposes.

If the estimation of the critical heat flux is of least importance for fire managers in case of large wildland fire spread, it is on the other hand of extreme importance before fire event in the following cases:

- *The control of fire spread through the wildland properties management:* this is done by planting fields of vegetation with low flammability and/or low heat release rate. Fuels of high moisture content can be good retardant of fire.
- *Fuel breaks at the wildland/urban interface:* the fuel break width is usually estimated so that fuels cannot be ignited on the urban side [60], because the heat flux is smaller than threshold flux for ignition. A critical heat flux obtained from deterministic methods would be over-estimated, and would allow probably fire initiation at the urban side. Thus, even weak, the initiated fire may be strengthened before fire fighters' intervention.

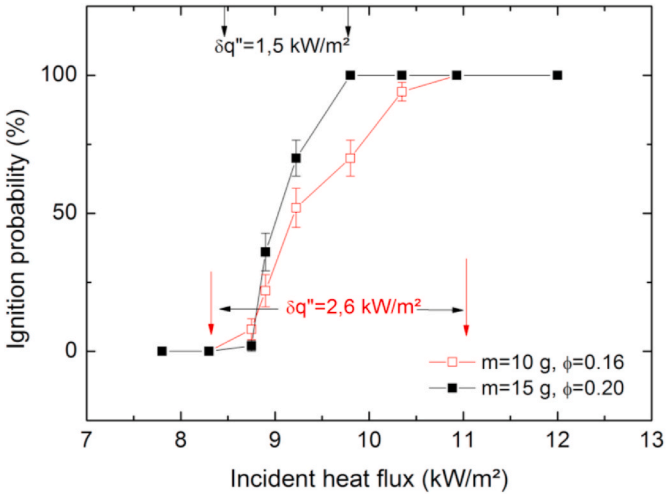

Fig. 4. Ignition probability for Ph needles (with errors) vs. incident heat flux. The arrows show the width of the transition region $\delta q''$.

A similar probabilistic ignition behavior as in Fig. 4 has been observed in the case of ignition of flammable liquids by hot surfaces [61]. It has been attributed to both the statistical nature of data and parametric variations in test conditions. It could be due to the heterogeneous air/fuel mixing process (fuel diffusion in flowing air). The width of the critical region of ignition probability for drop liquids could depend on the microscopic composition of the liquid fuel. In Fig. 4, the width ($\delta q''$) seems to decrease as the packing ratio increases. It would be interesting to investigate such a probabilistic aspect for solid fuels like PMMA, although cheaper solid fuels might be used for this end.

The rate of spread is one of the most used quantities by fire science community for wildland fires characterization. It corresponds to the inverse of ignition time, but the spread/non-spread transition is not only induced by the critical heat flux delivered by the flame but also by its residence time (combustion time). Fire spread is not possible if the residence time of the flame is smaller than the time required by the nearest fuel bed for its ignition, even if the heat release rate of burning fuel is larger than the critical heat flux for ignition. The flame residence time of burning fuels is finite (e.g. around 30 s for needles if arranged in non-compacted beds [62]) whereas the heat flux supplied by the cone calorimeter can be maintained until ignition. Zekri et al. [63] have distinguished this spreading transition (called dynamic transition) from that induced by the spatial heterogeneity of the fuel [6].

5. Conclusions

Ignition time of Mediterranean wildland fuels was measured using a cone calorimeter, and estimated analytically and numerically by means of a model based on energy balance. Although the model was widely used to describe ignition process and to predict wildland fire spread, it fails in estimating ignition time in the critical region. The main cause of this disagreement comes from the critical mass loss rate that misses from the ignition criteria used by the model. The critical heat flux for ignition was estimated for experimental data using a new method based on the power-law behavior of ignition time characterizing phase transitions. The threshold value of the flux was found much smaller than those mentioned in literature (e.g. for *Ph* needles), with fire safety consequences in many wildland fire situations. The discrepancy is explained by the probabilistic ignition behavior appearing in the critical region, which was ignored by the deterministic methods of literature. It is suggested that such a probabilistic behavior is due to the heterogeneities of fuel particles arrangement and even probably to those of the microscopic components flow and diffusion processes. This opens the question of assessing the probabilistic behavior for solid fuels ($\varphi = 1$).

CRediT authorship contribution statement

F.Z. Sabi: Software, Formal analysis, Writing - original draft, Visualization. **S.M. Terrah:** Formal analysis, Validation. **O. Mosbah:** Formal analysis, Validation. **A. Dilem:** Formal analysis, Validation. **N. Hamamousse:** Formal analysis, Validation. **A. Sahila:** Formal analysis, Validation. **O. Harrouz:** Formal analysis, Validation. **H. Boutchiche:** Formal analysis, Validation, Investigation. **F. Chaib:** Formal analysis, Validation, Investigation. **N. Zekri:** Formal analysis, Validation, Project administration, Funding acquisition, Writing - review & editing, Software, Data curation, Conceptualization, Methodology, Supervision, Writing, . **A. Kaiss:** Writing - review & editing, Formal analysis, Resources. **J.-P. Clerc:** Conceptualization, Data curation. **F. Giroud:** Resources, Formal analysis. **D.X. Viegas:** Writing - review & editing, Formal analysis, Validation.

Declaration of competing interest

There is no conflict of interest for this submission.

Acknowledgement

This work has been supported by the Algerian Direction Générale de la Recherche Scientifique et du Developpement Technologique under the framework of the FNRSDT, laboratory code W1030400.

Appendix

Let us demonstrate equation (18) using the above energy conservation equation (9), which can be rewritten as:

$$\begin{cases} \int_0^{t_1} [q''_{inc} - h_c(T-T_0)]dt + \\ \int_{t_1}^{t_1+t_2} [q''_{inc} - h_c(T-T_0)]dt + = \\ \int_{t_1+t_2}^{t_{ign}} [q''_{inc} - h_c(T-T_0)]dt \end{cases} \begin{cases} \int_{T_0}^{373K} \varphi(0)\rho(0)e\left[c_p^f + h_w c_p^w\right]dT - \\ \int_{h_w}^{0} \varphi(0)\rho(0)eL_w dh'_w + \\ \int_{373\ K}^{T_{pyr}} \varphi(0)\rho(0)ec_p^f dT \end{cases} \quad (A.1)$$

Ignition time is the sum of the 3 steps durations of (A.1): the heating up to boiling temperature ($T_0 \leq T < 373$ K) for a time span t_1, water evaporation for time span t_2, and dry fuel heating up to pyrolysis for time span t_{ign}-t_1-t_2. From (A.1), the differential equation of the first step is:

$$q''_{inc} - h_c(T-T_0) = \tau' h_c \frac{d(T-T_0)}{dt} \quad (A.2)$$

where the moist fuel relaxation time is $\tau' = \tau\left(1 + h_w \frac{c_p^w}{c_p^f}\right)$. The solution of (A.2) is:

$$T - T_0 = \frac{q''_{inc}}{h_c}\left(1 - e^{-\frac{t}{\tau'}}\right) \quad (A.3)$$

Replacing equation (A.3) in the first term of (A.1), the energy conservation for the first step yields:

$$\int_0^{t_1} q''_{inc} e^{-\frac{t}{\tau}} dt = \int_0^{373-T_0} \tau' h_c d(T-T_0) \tag{A.4}$$

This yields after integration:

$$q''_{inc}\left(1-e^{-\frac{t_1}{\tau}}\right) = Q''_c \tag{A.5}$$

Here $Q''_c = h_c(373 - T_0)$. The first step time t_1 is:

$$t_1 = \tau' \ln\left(1-\frac{Q''_c}{q''_{inc}}\right)^{-1} \tag{A.6}$$

Regarding the second step duration t_2 (water evaporation) $q''_{lost} = h_c(373 - T_0) = Q''_c$ and the energy conservation yields:

$$\int_{t_1}^{t_1+t_2} (q''_{inc} - Q''_c)dt = -\int_{h_w}^{0} \varphi(0)\rho(0)eL_w dh'_w = \int_0^{h_w} \tau \frac{L_w h_c}{c_p^f} dh'_w \tag{A.7}$$

Then:

$$t_2 = \tau h_w \frac{L_w h_c / c_p^f}{q''_{inc} - Q''_c} \tag{A.8}$$

The third step corresponds to pyrolysis of dry fuel in the temperature range $373\,K \le T < T_{pyr}$. Temperature solution is similar to equation (A.3) with a relaxation time $\tau = \varphi(0)\rho(0)ec_p^f/h_c$ instead of τ'. The energy conservation equation for the third step is then:

$$\int_{t_1+t_2}^{t_1+t_2+t_3} [q''_{inc} - h_c(T-T_0)]dt = \int_{373-T_0}^{T_{pyr}-T_0} \tau h_c d(T-T_0) \tag{A.9}$$

Here temperature exhibits a relaxation process as in (A.3) with a relaxation time τ. This yields after integration:

$$q''_{inc}\tau\left(e^{-\frac{t_1+t_2}{\tau}} - e^{-\frac{t_{ign}}{\tau}}\right) = \tau(q''_c - Q''_c) \tag{A.10}$$

With $q''_c = h_c(T_{pyr} - T_0)$. Rewriting $t_1 + t_2$ from equation (A.6) and equation (A.8) yields:

$$t_1 + t_2 = \tau\left(1 + h_w \frac{c_p^w}{c_p^f}\right)\ln\left(1-\frac{Q''_c}{q''_{inc}}\right)^{-1} + \tau h_w \frac{L_w h_c / c_p^f}{q''_{inc} - Q''_c} \tag{A.11}$$

Finally we have:

$$e^{-\frac{t_{ign}}{\tau}} = e^{-h_w \frac{L_w h_c / c_p^f}{q''_{inc} - Q''_c}}\left(1-\frac{Q''_c}{q''_{inc}}\right)^{1+h_w\frac{c_p^w}{c_p^f}} - \frac{(q''_c - Q''_c)}{q''_{inc}} \tag{A.12}$$

The logarithm of (A.12) yields equation (18)

$$t_{ign}/\tau = -\ln\left(e^{-h_w \frac{L_w h_c / c_p^f}{q''_{inc} - Q''_c}}\left(1-\frac{Q''_c}{q''_{inc}}\right)^{1+h_w\frac{c_p^w}{c_p^f}} - \frac{q''_c - Q''_c}{q''_{inc}}\right) \tag{A.13}$$

References

[1] H. Zhang, Fire-Safe Polymers and Polymer Composites, US Department of Transport, 2004. Report Number: DOT/FAA/AR-04/11.

[2] A.M. Grishin, V.P. Zima, V.T. Kuznetsov, A.I. Skorik, Ignition of combustible forest materials by a radiant energy flux, Combust. Explos. Shock Waves 38 (2002) 24–29, https://doi.org/10.1023/A:1014097631884.

[3] J.G. Quintiere, Fundamentals of Fire Phenomena, J.Wiley & Sons West Sussex, 2006.

[4] R.E. Lyon, J.G. Quintiere, Criteria for piloted ignition of combustible solids, Combust. Flame 151 (2007) 551–559, https://doi.org/10.1016/j.combustflame.2007.07.020.

[5] D. Drysdale, An Introduction to Fire Dynamics, third ed., A John Wiley & Sons, Ltd., Publication, 2011.

[6] D. Stauffer, A. Aharony, Introduction to Percolation Theory, Taylor and Francis, London, 1992.

[7] S.J. Blundell, K.M. Blundell, Concepts in Thermal Physics, Oxford University Press, Oxford, 2006.

[8] H.E. Stanley, Introduction to Phase Transitions and Critical Phenomena, Clarendon Press Oxford, 1971.

[9] V.L. Pokrovskii, Two-dimensional magnetic phase transitions, J. Magnetism and Magnetic materials 200 (1999) 515–531, https://doi.org/10.1016/S0304-8853(99)00406-0.

[10] J.M. Yeomans, Statistical Mechanics of Phase Transitions, Clarendon Press, Oxford, 1992.

[11] P. Mindykowski, P. Fuentes, J.L. Consalvi, B. Porterie, Piloted ignition of wildland fuels, Fire Saf. J. 46 (2011) 34–40, https://doi.org/10.1016/j.firesaf.2010.09.003.

[12] M.M. Khan, J.L. DeRis, S.D. Ogden, Effect of moisture on ignition time of cellulosic materials, Fire Saf. Sci. Proc. Ninth Int. Symp. 9 (2008) 167–178, https://doi.org/10.3801/IAFSS.FSS.9-167.

[13] V. Babrauskas, Ignition of wood: a review of the state of the art, J.Fire Prot. Eng. 12 (2002) 163–189, https://doi.org/10.1177/10423910260620482.

[14] I. Vermesi, M.J. DiDomizio, F. Richter, E.J. Weckman, G. Rein, Pyrolysis and spontaneous ignition of wood under transcient irradiation: experiments and a-priori predictions, Fire Saf. J. 91 (2017) 218–225, https://doi.org/10.1016/j.firesaf.2017.03.081.

[15] ASTM International, Designation E 1354-17, Standard Test Method for Heat and Visible Smoke Release Rates for Materials and Products Using an Oxygen Consumption Calorimeter .

[16] N. Bal, G. Rein, Numerical investigation of the ignition delay time of a translucent solid at high radiant heat fluxes, Combust. Flame 158 (2011) 1109–1116, https://doi.org/10.1016/j.combustflame.2010.10.014.

[17] J.G. Quintiere, M. Harkleroad, New Concepts for Measuring Flame Spread Properties, National Bureau of Standards, Gaithersburg, MD NBSIR, 1984, 84-2943.

[18] E. Mikkola, I. Wichman, On the thermal ignition of combustible materials, Fire Mater. 14 (1989) 87–96, https://doi.org/10.1002/fam.810140303.

[19] M. Delichatsios, Y. Chen, Asymptotic, approximate, and numerical solutions for the heatup and pyrolysis of materials including reradiation losses, Combust. Flame 92 (1993) 292–307, https://doi.org/10.1016/0010-2180(93)90041-Z.

[20] M. Dietenberger, Ignitability analysis using the cone calorimeter and LIFT apparatus, Proceedings of the International Conference on Fire Safety 22 (1996) 189–197. Columbus, OH.

[21] A.P. Demitrakopoulos, K.K. Papaioannou, Flammability assessment of Mediterranean forest fuels, Fire Technol. 37 (2001) 143–152, https://doi.org/10.1023/A:1011641601076.

[22] G.M. Byram, Combustion of forest fuel, in: K.P. Davis (Ed.), Forest Fire: Control and Use, McGraw-Hill, New York, 1959, pp. 61–89.

[23] P. Ciccioli, M. Centritto, F. Loreto, Biogenic organic volatile compound emissions from vegetation fires, Plant Cell Environ. 37 (2014) 1810–1825, https://doi.org/10.1111/pce.12336.

[24] R.C. Rothermel, A Mathematical Model for Predicting Fire Spread in Wildland Fuels, USDA, 1972, p. 40. For.Serv.Res. Pap. INT-115.

[25] S.M. Terrah, F.Z. Sabi, O. Mosbah, A. Dilem, N. Hamamousse, A. Sahila, O. Harrouz, H. Boutchiche, F. Chaib, N. Zekri, A. Kaiss, J.P. Clerc, F. Giroud, D. X. Viegas, Nonexistence of critical fuel moisture content for flammability, Fire Saf. J. 111 (2020), 102928, https://doi.org/10.1016/j.firesaf.2019.102928.

[26] M.J. DiDomizio, P. Mulherin, E.J. Weckman, Ignition of wood under time-varying radiant exposures, Fire Saf. J. 82 (2016) 131–144, https://doi.org/10.1016/j.firesaf.2016.02.002.

[27] J.K. Adou, Y. Billaud, D.A. Brou, J.P. Clerc, J.L. Consalvi, A. Fuentes, A. Kaiss, F. Nmira, B. Porterie, L. Zekri, N. Zekri, Simulating wildfire patterns using a small-world network model, Ecological Modeling 221 (2010) 1463–1471, https://doi.org/10.1016/j.ecolmodel.2010.02.015.

[28] P. Koo, P. Pagni, P. Woycheese, S. Stephens, D. Weise, J. Huff, A simple physical model for forest fire spread rate, Fire Saf. Sci. Proc. Eight Int. Symp. (2005) 851–862.

[29] P. Boulet, G. Parent, Z. Acem, A. Collin, M. Försth, N. Bal, G. Rein, J. Torero, Radiation emission from a heating coil or a halogen lamp on a Semi-transparent sample, Int. J. Therm. Sci. 77 (2014) 223–232, https://doi.org/10.1016/j.ijthermalsci.2013.11.006.

[30] G. Rein, Smoldering combustion, in: M.J. Hurley (Ed.), SFPE Handbook of Fire Protection Engineering, Springer, Heidelberg, 2016, pp. 581–603, chap.19.

[31] I. Vermesi, N. Roenner, P. Pironi, R.M. Hadden, G. Rein, Pyrolysis and ignition of a polymer by transient irradiation, Combust. Flame 163 (2016) 31–41, https://doi.org/10.1016/j.combustflame.2015.08.006.

[32] P. Reszka, P. Borowiec, T. Steinhaus, J.L. Torero, A methodology for the estimation of ignition delay times in forest fire modelling, Combust. Flame 159 (2012) 3652–3657, https://doi.org/10.1016/j.combustflame.2012.08.004.

[33] V. Babrauskas, Ignition of Wood: A Review of the State of the Art, Interflam Interscience Communications Ltd., London, 2001, pp. 71–88.

[34] V. Tihay-Felicelli, P.A. Santoni, T. Barboni, L. Leonelli, Autoignition of dead shrub twigs: influence of diameter on ignition, Fire Technol. 52 (2016) 897–929, https://doi.org/10.1007/s10694-015-0514-x.

[35] W. Wagner, H.J. Kretzschmar, Properties of water and steam, in: VDI Heat Atlas, Springer-Verlag, Berlin Heidelberg 2nd ed., 2010, p. 154.

[36] P.S. Lam, S. Sokhansanj, X. Bi, C.J. Lim, L.J. Naimi, M. Hoque, S. Mani, A. R. Womac, X.P. Ye, S. Narayan, Bulk density of wet and dry wheat straw and switchgrass particles, Appl. Eng. Agric. 24 (2008) 351-358, https://doi.org/10.13031/2013.24490.

[37] H.K. Ahn, T.J. Sauer, T.L. Richard, T.D. Glanville, Determination of thermal properties of composting bulking materials, Bioresour. Technol. 100 (2009) 3974–3981, https://doi.org/10.1016/j.biortech.2008.11.056.

[38] A. Lamorlette, M. El Houssami, J.C. Thomas, A. Simeoni, D. Morvan, A dimensional analysis of forest fuel layer ignition model: Application to the ignition of pine needle litters, J. Fire Sci. 33 (2015) 320–335, https://doi.org/10.1177/0734904115591177.

[39] E.M. Okonkwo, J.O. Odigure, J.O. Ugwu, K. Mu'azu, I.S. Williams, B.E. Nwobi, F. K. Okoriel, V.N. Oriah, Design of pilot plant for the production of essential oil from Eucalyptus leaves, J. Sci. Ind. Res. 65 (2006) 912–915. http://hdl.handle.net/123456789/4957.

[40] S. Cavagnol, Approche multi-échelle de l'emballement des réactions exothermiques de torréfaction de la biomasse ligno-cellulosique de la cinétique chimique au lit de particules. Phd thesis, École Centrale Des Arts Et Manufactures, 2013 (see also the references therein).

[41] J.P. Bouchaud, Anomalous relaxation in complex systems: from stretched to compressed exponentials anomalous transport, in: R. Klages, G. Radon, I. M. Sokolov (Eds.), Anomalous Transport: Foundations and Applications, Wiley Weinheim, 2008.

[42] A. Stanislavski, K. Weron, Fractional calculus tools applied to study the nonexponential relaxation in dielectrics, in: V.E. Tarasov (Ed.), Handbook of Fractional Calculus with Applications in Physics, De Gruyter Berlin, 2019.

[43] D. Alexandrian, E. Rigolot, Sensibilité du pin d'Alep à l'incendie, Forêt méditerranéenne 3 (1992) 185–198. http://hdl.handle.net/2042/40447.

[44] M. Häusler, J.P. Nunes, P. Soares, J.M. Sánchez, J.M.N. Silva, T. Warneke, J. J. Keizer, J.M.C. Pereira, Assessment of the indirect impact of wildfire (severity) on actual evapotranspiration in eucalyptus forest based on the surface energy balance estimated from remote-sensing techniques, Int. J. Rem. Sens. 39 (2018) 6499–6524, https://doi.org/10.1080/01431161.2018.1460508.

[45] S.J. Pyne, P.L. Andrews, R.D. Laven, Introduction to Wildland Fire, Wiley, New York, 1996.

[46] B. Gabbert, Eucalyptus and fire, Wildfire today, March 3,, https://wildfiretoday.com/2014/03/03/eucalyptus-and-fire/, 2014.

[47] J.L. Torero, A. Simeoni, Heat and mass transfer in fires: scaling laws, ignition of solid fuels and application to forest fires, Open Therm. J. 4 (2010) 145–155, https://doi.org/10.2174/1874396X01004010145.

[48] C. Beyler, Flammability limits of premixed and diffusion flames, in: M.J. Hurley (Ed.), SFPE Handbook of Fire Protection Engineering, Springer, Heidelberg, 2016, pp. 529–553, chap.17.

[49] N. Hamamousse, H. Boutchiche, Etude des surfaces de végétation par microscopie électronique à balayage, LEPM, private communication, 2018.

[50] D.X. Viegas, J. Raposo, D. Davim, C. Rossa, Study of the jump fire produced by the interaction of two oblique fire fronts. Part 1. Analytical model and validation with no-slope laboratory experiments, Int. J. Wildland Fire 21 (2012) 843–856, https://doi.org/10.1071/WF10155.

[51] J.R. Raposo, D.X. Viegas, X. Xie, M. Almeida, A.R. Figueiredo, L. Portoand, J. Sharples, Analysis of the physical processes associated with junction fires at laboratory and field scales, Int. J. Wildland Fire 27 (2018) 52–68, https://doi.org/10.1071/WF16173.

[52] R.T. Toledo, Fundamentals of Food Process Engineering, third ed., Springer Science Business Media, LLC., 2007, p. 579.

[53] L. Courty, K. Chetehouna, L. Lemée, C. Fernandez-Pello, J.-P. Garo, Biogenic volatile organic compounds emissions at high temperatures of common plants from mediterranean regions affected by forest fires, J. Fire Sci. 32 (2014) 459–479, https://doi.org/10.1177/0734904114536128.

[54] R.M. Hadden, S. Scott, C. Fernandez-Pello, Ignition of combustible fuel beds by hot particles: an experimental and theoretical study, J. Fire Technology 47 (2011) 341–355, https://doi.org/10.1007/s10694-010-0181-x.

[55] J.W. Van Wagtendonk, Fire as a physical process, in: Sugihara, et al. (Eds.), Fire in California's Ecosystems, University of California Press, California, 2006, https://doi.org/10.1525/california/9780520246058.003.0003. Chapter: 3.

[56] L. Shi, M.Y.L. Chew, Experimental study of woods under external heat flux by autoignition:Ignition time and mass loss rate, J. Therm. Anal. Calorim. 111 (2012) 1399–1407, https://doi.org/10.1007/s10973-012-2489-x.

[57] I. Vermesi, N. Roenner, G. Rein, Blind Predictions of Polymer Pyrolysis and the Dual Threshold for Ignition, Imperial Hazelab Repository, 2017, https://doi.org/10.5281/zenodo.3228479.

[58] L.D. Landau, E.M. Lifshitz, Statistical Physics, Pergamon Press, Toronto, 1970, p. 343.

[59] J.W. Lindeberg, Eine neue Heirleitung des Exponentialgesetzes in der Wahrscheinlichkeitsrechnung, Math. Z. 15 (1922) 211–225. http://www.digizeitschriften.de/dms/img/?PID=GDZPPN002367076.

[60] A. Kaiss, L. Zekri, N. Zekri, B. Porterie, J.-P. Clerc, C. Picard, Efficacité des coupures de combustible dans la prévention des feux de forêt, C.R.Physique 8 (2007) 462–468, https://doi.org/10.1016/j.crhy.2007.02.002.

[61] J.D. Colwell, A. Reza, Hot surface ignition of automotive and aviation fluids, J. Fire Technology 41 (2005) 105–123.

[62] B.M. Wotton, J.S. Gould, W.L. MacCaw, N.P. Cheney, S.W. Taylor, Flame temperature and residence time of fires in dry eucalypt forest, Int. J. Wildland Fire 21 (2012) 270–281, https://doi.org/10.1071/WF10127.

[63] N. Zekri, B. Porterie, J.P. Clerc, J.C. Loraud, Propagation in a two-dimensional weighted local small-world network, Phys. Rev.E 71 (2005), 046121, https://doi.org/10.1103/PhysRevE.71.046121.